73rd International Astronautical Congress (IAC), Paris, France, 18-22 September 2022.

IAC-22-C1.7.3

Binary Asteroid Landing Trajectory Design from a Self-Stabilized Terminator Orbit Considering Parametric Uncertainties.

Iosto Fodde[1, a], Jinglang Feng[1, b], Jesús Gil-Fernández[2, c], Massimiliano Vasile[1, d]

[1] *Department of Mechanical and Aerospace Engineering, University of Strathclyde, 75 Montrose Street, Glasgow G1 1XJ, United Kingdom.*

[2] *Systems Department, Guidance, Navigation and Control Section (TEC-SAG), European Space Agency, Keplerlaan 1, P.O. Box 299, 2200 AG Noordwijk, The Netherlands.*

[a] *iosto.fodde@strath.ac.uk.*

[b] *jinglang.feng@strath.ac.uk.*

[c] *jesus.gil.fernandez@esa.int.*

[d] *massimiliano.vasile@strath.ac.uk.*

Abstract

The landing of probes on minor solar system bodies allows for in depth analyses on the formation and evolution of these types of bodies. Due to the long descent time and highly non-linear environment, a minor body landing trajectory can be highly sensitive to uncertainties in the deployment state and environment parameters. In this research, a method to design robust ballistic landing trajectories is introduced and applied to the case of Didymos. Specifically, the landing trajectory is initiated from a self-stabilized terminator orbit (SSTO) and lands on the surface of the secondary body Dimorphos. Starting from a range of allowable landing conditions and uncertainties in the gravitational fields of the bodies, a set of trajectories together with its uncertainties is propagated backwards in time using the generalised intrusive polynomial algebra method until it intersect with the SSTO. This solution is then refined using a grid search together with the non-intrusive Chebyshev interpolation method to propagate the uncertain state forward in time. It is shown that the trajectory found with this technique is able to improve the landing success percentage by 26 percent compared to conventional methods. The approach developed in this work allows for the design of ballistic trajectories under uncertainties, and increases the safety and feasibility of these types of missions.

Keywords: Didymos System, Uncertainty Analysis, Ballistic Landing, Trajectory Design

1 Introduction

Planned for late September 2022, NASA's Double Asteroid Redirection Test (DART) will impact the secondary body of binary asteroid system Didymos to test the ability of a kinetic impactor to redirect an asteroid. This mission is part of the Asteroid Impact and Deflection Assessment (AIDA) collaboration between NASA and ESA, where ESA will send its spacecraft, Hera, to investigate the result of DART's impact in more detail. After arrival, two CubeSats on board Hera will be released around the system, ending with a landing on the secondary Dimorphos [1]. During this landing, several instruments on-board the CubeSats will measure the internal structure from the bouncing motion and do some in-situ measurements to characterize Dimorphos and the result of DART's impact in more detail.

Similar landings can be found for the Hayabusa mission [2], Rosetta [3], Hayabusa 2 [4], and OSIRIS-REx [5]. The requirements on the guidance, navigation, and control (GNC) system for precise landings are quite stringent and could add a significant amount of complexity to the design of the CubeSats. Therefore, ballistic landings, i.e. with no active control of the translational state during descent, are good options for the landing maneuver as this reduces the complexity of the GNC system. Specifically, as CubeSats have limited mass and volume budgets, the extra ΔV and GNC sensors and actuators that are required for the active descent option can have a large impact. Therefore, the ballistic landing trajectory option is preferable. However, the problem with ballistic landing trajectories is that they are more sensitive to errors in the deployment maneuver and uncertainties in the dynamical parameters [6]. Thus, the design of the landing trajectory needs to account for this to increase the likelihood of a successful landing.

The dynamics governing the landing on the secondary of a binary asteroid system can be complex due to the low gravitational forces and the large influence of the pri-

mary body. In [7], favourable ballistic landing trajectories were constructed using the hyperbolic manifolds around the L_2 Lagrange point. Uncertainties were also considered for this specific maneuver in [8], which showed that for the deployment from L_2, this approach can be quite robust. This work was further extended to deployment from certain periodic orbits, e.g. terminator orbits, near the L_2 point [9]. Additionally, [10] looked at the change of these hyperbolic manifolds used for landing when considering non-spherical gravitation perturbations and different rotational rates. It was found that these parameters have a significant impact on the amount of trajectories being able to land on the surface. Extending to general deployment points beyond the L_2 point, [11] developed a bisection based method to find minimum touchdown velocity landing trajectories for any landing location on the body. The implementation of an uncertainty propagation technique to improve the robustness of this technique was performed in [12]. The specific investigation for ballistic landing trajectories specifically on the secondary of the Didymos system has seen an increase in interest in recent years due to the Hera mission, see e.g. [13] and [14].

For this work, a landing trajectory specifically from a Self-Stabilized Terminator Orbit (SSTO) is considered. This requires an adaptation of the techniques discussed in the previous works. This type of orbit was found to be stable in case of a relative large influence of the Solar Radiation Pressure (SRP) force [15], and thus are desirable options for the operational orbits of the CubeSats [1]. For regular landing trajectory design, first a nominal model is used to find trajectories that (locally or globally) minimize a certain objective function. Then, the sensitivity of the solution is tested against both initial state uncertainties and dynamical model uncertainties, also called parametric uncertainties. The solution is then adjusted to reduce the sensitivity to the uncertainties in case the requirements are not met anymore. In case of large uncertainties, or very sensitive systems, this approach might fail as the most robust solution might differ significantly from the nominal optimal solution [16]. This can be shown graphically in figure 1, where d is the objective, x the decision variable, and β some model parameter. In case of uncertainties in x_1 or β_1, the value for the optimal solution d_1 can possible change by a large amount as the distribution of d due to $\Delta x_1/\Delta\beta_1$ is spread out over a large range of values. Whereas for the solution corresponding to d_2, the value does not change significantly due to the uncertainties in x_2 or β_2. Therefore, d_2 might be more desirable at it is more robust even if it increases the minimum possible value of d. An example of robust trajectory design for landing on an asteroid using active control during descent can be found in [17].

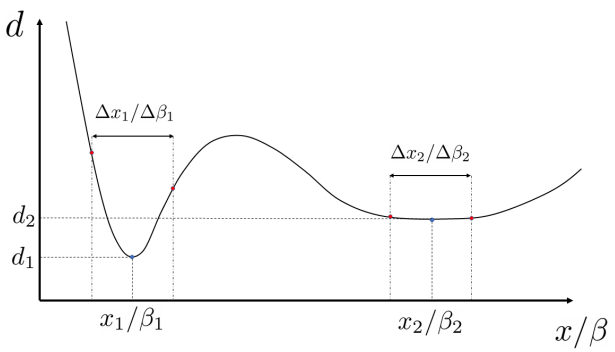

Figure 1: Diagram explaining the concept of finding a robust trajectory. Trajectory 1 nominally has the best value for the objective d. However, when adding the uncertainty in the state x or model parameter β, the change Δ in these values can cause a large increase in d. Trajectory 2 has a lower nominal value for d, but is less sensitive to changes in x and/or β, thus is more robust.

In this work, the design of a robust ballistic landing trajectory from a SSTO is considered. A technique to find several possible robust trajectories is discussed and an example of one of these trajectories is shown as well. This paper is structured as follows: first the dynamical system is discussed in section 2. Second, the uncertainty propagation techniques necessary for this work are explained in section 3. Afterwards, section 4 introduces the method to find an initial guess for the robust landing trajectory. Finally, section 5 discusses the final step for the trajectory solution and 6 states the conclusions of this work.

2 Binary Asteroid Dynamics

The Didymos (68503) binary system consists of two seperate bodies, the 780 meter diameter primary called Didymos and the 164 meter secondary Dimorphos. Some of the relevant physical properties of the binary system coming from recent observations can be found in Table 1. The circular restricted three-body problem (CR3BP) is applied to model the system, as Dimorphos is in a nearly circular planar orbit around Didymos, and the mass of the CubeSat is negiligible compared to the mass of the two asteroids. For the equations of motion in the CR3BP, a synodic reference frame that rotates together with the orbit of Dimorphos is considered. The origin of this frame is

Table 1: Relevant physical parameters of the Didymos system, taken from [18].

Parameter	Value and Uncertainty
System mass	5.28 ($\pm$ 0.54) $\cdot 10^{11}$ kg
Mass ratio	0.0093 $\pm$ 0.0013
Didymos Diameter	780 m $\pm$ 3 m
Didymos Rotational Period	2.26 h $\pm$ 0.0001 h
Dimorphos Diameter	164 m $\pm$ 18 m
Dimorphos Orbital Period	12 h
Body separation distance	1.19 km

located in the barycentre of the system, the x-axis points towards Dimorphos, the z-axis to the orbit normal, and the y-axis completes the right-handed frame.

The dynamics of the CubeSats in the synodic frame can be formulated as follows [19]:

$$\ddot{x} - 2\dot{y} = \frac{\partial U}{\partial x}, \tag{1}$$

$$\ddot{y} + 2\dot{x} = \frac{\partial U}{\partial y}, \tag{2}$$

$$\ddot{z} = \frac{\partial U}{\partial z}. \tag{3}$$

Here, x, y, and z are dimensionless parameters, where the mass parameter $\mu = m_2/(m_1 + m_2)$, the body separation distance R, and the time constant $1/n$ (where n is the mean motion of Dimorphos) were used to obtain them. This also significantly simplifies the equations as they now only depend on the mass parameter μ and the dimensionless state variables. The potential U includes both the rotational terms stemming from the non-inertial reference frame used, and the gravitational forces acting on the third body. For the close proximity motion that is considered here, the gravitational forces from both asteroids dominate the dynamics compared to other forces like the Solar radiation pressure or the Solar gravity [20]. Thus, only these forces are considered. The uncertainties in the gravitational forces considered in this work stem from both the estimation of the physical properties and the accuracy of the dynamical models. Therefore, a simple and more numerically efficient point mass gravity model is used, and the lower accuracy of this model compared to e.g. a polyhedron gravity model, is accounted for in the size of the uncertainties. The specific effect of non-spherical gravity and its uncertainty on the landing trajectory can still have some impact on the trajectory design process, and are thus left for future work. The potential U in the case considered here is given by:

$$U = \frac{1}{2}(x^2 + y^2) + \frac{1-\mu}{r_1} + \frac{\mu}{r_2}, \tag{4}$$

where r_1 and r_2 represent the distance from the spacecraft to the primary and secondary, respectively.

The CR3BP allows an integral of motion called Jacobi's constant, given by [19]:

$$C = 2U - V^2, \tag{5}$$

where V is the velocity of the 3rd body. This variable can be seen as an energy measure, where lower values correspond to higher energy spacecraft trajectories. Constant values of $C = 2U$ give surfaces where the velocity of the spacecraft is zero and are called zero-velocity surface (ZVS).

It is expected that the impact of DART will result in potentially significant changes to both the physical state of Dimorphos and its translational and rotational motion [21]. As it is difficult to predict these changes beforehand, the current estimates will be used in the dynamical modelling of the system. The uncertainties considered in this work can be assumed to stem from both the current observations and the physical mis-modelling due to the DART impact. The implementation and analysis of the effect of these uncertainties on the landing design process is out of the scope of this work.

3 Uncertainty Propagation

Consider an initial value problem defined as follows:

$$\begin{cases} \dot{\boldsymbol{x}} = \boldsymbol{f}(\boldsymbol{x}(t), \boldsymbol{\beta}, t) \\ \boldsymbol{x}(t_0) = \boldsymbol{x}_0 \end{cases} \tag{6}$$

where t is the time, $\boldsymbol{x}$ is the state vector, and $\boldsymbol{\beta}$ is the dynamical model parameters. If the initial state $\boldsymbol{x}_0$ and model parameters β are uncertain, a set of N realisation or samples can be taken as follows: $[\boldsymbol{x}_{0,1}, \boldsymbol{\beta}_1, ..., \boldsymbol{x}_{0,N}, \boldsymbol{\beta}_N]$. Propagating each sample through Eq.(6) until time t_f results in the trajectories $\boldsymbol{x}_i(t_f) = \phi_i(\boldsymbol{x}_{0,i}, \boldsymbol{\beta}_i, t_f)$.

The set of all possible initial states is given as follows:

$$\Omega_{\boldsymbol{x}_0} = \{\boldsymbol{x}(t_0, \boldsymbol{\xi}) \mid \boldsymbol{\xi} \in \Omega_{\boldsymbol{\xi}}\}. \tag{7}$$

Where $\boldsymbol{\xi} = [\boldsymbol{x}_0, \boldsymbol{\beta}]$. This set can be propagated up until a specific time t to obtain the set:

$$\Omega_t(\boldsymbol{\xi}) = \{\boldsymbol{x}(t) = \phi(\boldsymbol{\xi}, t) \mid \boldsymbol{\xi} \in \Omega_{\boldsymbol{\xi}}\}. \tag{8}$$

This set represents all possible trajectories at time t from the realisations of the uncertainty vector $\boldsymbol{\xi}$ within the uncertainty set $\Omega_{\boldsymbol{\xi}}$. Therefore, to understand the effect of the uncertainties on this system, an analytical expression of this set needs to be obtained.

If $\boldsymbol{x}_t$ is continuous in $\boldsymbol{\xi}$ and the set is compact, $\Omega_t(\boldsymbol{\xi})$ can be approximated using a polynomial function:

$$\tilde{\Omega}_t(\boldsymbol{\xi}) = P_{n,d}(\boldsymbol{\xi}) = \sum_{i=0}^{\mathcal{N}} c_i(t)\alpha_i(\boldsymbol{\xi}), \tag{9}$$

where $\alpha_i(\boldsymbol{\xi})$ are a set of multivariate polynomial basis functions, $c_i(t)$ are the corresponding coefficients, and $\mathcal{N} = \binom{n+d}{d}$ is the number of terms of the polynomial, where n is the degree of the polynomial and d is the number of variables. There are various option to obtain the polynomial of function (9). Two different techniques are used in this work. The first method is an intrusive technique called the generalised intrusive polynomial algebra (GIPA) [22]. Besides this intrusive method, a non-intrusive Chebyshev interpolation (NCI) [23] method is also used here. Both these methods are discussed in the following sections.

3.1 Generalised Intrusive Polynomial Algebra

The GIPA technique is a generalisation of several techniques based on higher order expansions of the flow using Taylor polynomials, like Differential Algebra [24] or Jet Transport [25]. In GIPA, a specific polynomial basis α is selected and used to approximate the initial set $\Omega_{\boldsymbol{x}_0}$. To be able to propagate this set using the dynamics specified by $\boldsymbol{f}(\boldsymbol{x}(t), \boldsymbol{\beta}, t)$ in Eq. (6), the space of polynomials $\mathcal{P}_{n,d}(\alpha)$ needs to be equipped with a set of elementary arithmetic operations. This enables the use of (numerical) integrators to propagate the polynomial function. In GIPA, instead of defining a specific set of operations for each different polynomial basis, a change of basis is performed to a monomial basis ϕ. Its main advantage is that it significantly reduces the computational cost and makes sure that only one set of elementary arithmetic operations needs to be implemented.

A set of elementary functions, $\otimes$, corresponding to similar operations in a floating point algebra, $\oplus \in \{+, -, \cdot, /\}$, is combined with the function space $\mathcal{P}_{n,d}(\phi)$ to create an algebra. Then, given any two functions f_a and f_b, and their polynomial approximations F_a and F_b, the same operations between the two functions in the floating point algebra can be represented in the polynomial algebra:

$$f_a \oplus f_b \sim F_a \otimes F_b. \tag{10}$$

Besides the set of elementary operations, a set of elementary functions $h(y)$, e.g. $\{1/y, \sin(y), \exp(y), \log(y), \text{etc.}\}$, needs to be represented in the algebra as well. This can be done using the composition operator as follows:

$$h(\boldsymbol{f}(\boldsymbol{x})) \sim H(y) \circ F(\boldsymbol{x}), \tag{11}$$

where $H(y)$ is the univariate polynomial representation of $h(y)$ and $F(\boldsymbol{x})$ the polynomial algebra representation of the multivariate set $\boldsymbol{f}(\boldsymbol{x})$. The composition operator is defined as follows:

$$\circ : \mathcal{P}_{n,1}(\phi) \times \mathcal{P}_{n,d}(\phi) \to \mathcal{P}_{n,d}(\phi). \tag{12}$$

Compared to the elementary operations, the polynomial approximation of the elementary functions $H(y)$ differs between the chosen polynomial bases. In [12] the accuracy of different polynomial bases for landing trajectories on Dimorphos were tested. From this analysis, the Chebyshev polynomial basis is selected for this work as it provides accurate results and is defined over a closed set. It was shown in [22] that a range estimation techniques is needed for the Chebyshev basis. It was shown that a coefficient based range estimation method results in an overestimation of the range, which decreases the overall accuracy. A sampling based method does not suffer from this drawback, however it is less efficient compared to the coefficient based method as a number of samples need to be taken from the polynomial function. For this work, the sample based range method is selected as an accurate representation of the state is needed to obtain feasible landing trajectories.

The basic process of using GIPA for uncertainty propagation is now as follows. First a polynomial approximation is taken over the uncertain variables at the initial time using the Chebyshev basis. This basis is then

transformed to the monomial basis to be able to use the general set of elementary operations, while using the elementary function approximation methods of Chebyshev polynomial basis. Using the desired numerical integrator, e.g. Runge-Kutta 4, the set can be propagated to the final desired time, using the algebra to replace each elementary operation and elementary function in the integrator and dynamical system. The convenience of this method is that no significant changes need to be made to the implementation of the methods that are normally used to propagate a single trajectory, as only the elementary operations and functions need to be replaced, which can be done in several different coding languages by overloading the operations. Here, the SMART-UQ package is used for this [26], which contains implementations of the algebra for various different polynomial bases.

3.2 Non-Intrusive Chebyshev Interpolation

For non-intrusive methods, the dynamics are treated as a black box. A set of input points are taken, and propagated through the dynamical system to obtain a set of responses. These responses can then be analysed in several different manners to get a better idea of the relation between the inputs and responses. The most basic and often used method is the Monte Carlo technique, where a large number of randomly sampled inputs are taken and the sample-based statistics are used to analyse the system. For an infinite amount of samples, the system can be represented perfectly. However, practically this is not possible and a finite set of points are used. To obtain convergence, often a large number of samples are required, which can become computationally expensive, and determining the necessary amount of samples can also be non-trivial [27].

Recent works (see e.g. [23], [28]) have shown that it is possible to find an analytical approximation of the dynamical response as a function of the input using polynomials. These polynomials can be constructed using significantly less points and information on the dynamical system can be obtained through the coefficients [29]. A multivariate Chebyshev polynomial basis is used here as its interpolation characteristics allow for uniform convergence, even in case of large uncertainties.

The coefficients of the polynomial shown in Eq. (9), where α is chosen to be the Chebyshev polynomial basis T, can be obtained by solving the following equations:

$$HC = Y, \tag{13}$$

where:

$$H = \begin{bmatrix} T_{i_1}(\boldsymbol{\xi}_1) & \dots & T_{i_s}(\boldsymbol{\xi}_1) \\ \vdots & \ddots & \vdots \\ T_{i_1}(\boldsymbol{\xi}_s) & \dots & T_{i_s}(\boldsymbol{\xi}_s) \end{bmatrix}, C = \begin{bmatrix} c_{i_1} \\ \vdots \\ c_{i_s} \end{bmatrix}, Y = \begin{bmatrix} y_1 \\ \vdots \\ y_s \end{bmatrix} \tag{14}$$

where $s = \mathcal{N} = \binom{n+d}{d}$, $\boldsymbol{\xi}_1, \dots, \boldsymbol{\xi}_s$ are the interpolation points, and Y the vector containing all the corresponding propagated samples $y_i = \phi_i(\boldsymbol{\xi}_i, t)$. The interpolation points are chosen according to a Latin Hypercube Sampling (LHS) method, which divides the sampling space into several subspaces in which a random sample is taken for each individual subspace. Other sampling methods like the Smolyak sparse grid more efficiently use the properties of Chebyshev interpolation polynomials and thus are able to improve the accuracy. However, they are more complex to implement and are thus left for future work.

4 Initial Trajectory Generation

The goal of this work is to generate a robust landing trajectory from a Self-Stabilized Terminator Orbit (SSTO) to the surface of the moon Dimorphos. A general set of requirements can be set for this trajectory, which are derived from e.g. [9] and [11]. Namely, the maximum impact velocity should be below 10 cm/s, the impact angle should be below 30 $\deg$, and the maximum deployment ΔV from the SSTO should be below 20 cm/s. As there are a large possible set of decision parameters (e.g. the deployment point along the SSTO, the relative phase with respect to Dimorphos, and the ΔV direction and magnitude), with a wide range of possible values, it is important to reduce the search area by obtaining an appropriate initial guess for the landing trajectory.

Similar to the technique from [12], a backwards propagation method is used to find sets of trajectories that originate from the surface of the asteroid and intersect with the SSTO. This process is shown graphically in Figure 2. For a certain desired landing location, velocity, and direction, a polynomial representing the set of landing states can be initialized as in Eq. (7). This set can then be propagated backwards in time, i.e. from the time of landing to the deployment time, using the GIPA technique. At each point in time, the minimum distance, $d^\star$, between the mean of the lander position set $\mu(\boldsymbol{x}_{land})$ and the mean of the SSTO position set $\mu(\boldsymbol{x}_{orb})$ is measured. If it is assumed that the SSTO is close to a circle in the y-z plane with nominal ra-

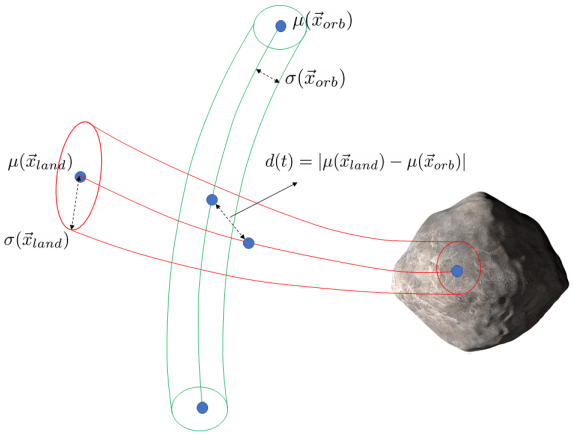

Figure 2: Diagram explaining the intersection between the orbiter and lander trajectory considering the uncertainties in the state.

dius $R = 2$ km, a simple formula for $d^\star$ and true anomaly, u, corresponding to the closest point is given by [30]:

$$d^\star = \sqrt{\bar{y}_{orb}^2 + \bar{z}_{orb}^2} - R, \tag{15}$$

$$u = \arctan\left(\frac{\bar{z}_{orb}}{\bar{y}_{orb}}\right). \tag{16}$$

If the distance is small enough, the variance of the lander set, $\sigma(\boldsymbol{x}_{land})$, can be used to define a region of possible deployment maneuvers from the SSTO. The mean and variance of the two sets can be calculated from the coefficients of the polynomial approximation of the state, as is shown in [29]. A high overlap between the SSTO and lander position sets corresponds to a high density of possible deployment maneuvers that allow for landing on Dimorphos. As the polynomial algebra allows for the calculation of the set of required $\Delta\boldsymbol{V}$ vectors, which correspond to all the possible maneuvers between the SSTO and lander sets, the lower and upper bounds on the $\Delta\boldsymbol{V}$ can be determined from this polynomial.

A grid search in the landing velocity magnitude, impact azimuth angle, and impact elevation angle is performed. For each grid point, the landing location is kept constant (at $-90\,\mathrm{deg}$ longitude and $0\,\mathrm{deg}$ latitude), with an allowable landing footprint of $5\,\mathrm{deg}$ in all directions. Together with this state uncertainty, an uncertainty of 10% is also introduced in the gravitational parameters of both Didymos and Dimorphos. This uncertainty allows for robustness of the landing trajectory not only against deployment errors but also against modelling errors. For each of these grid points, the minimum distance along the landing trajectory $d^\star$ and the upper bound of the magnitude of the $\Delta\boldsymbol{V}$ is calculated.

A Pareto front is generated from the grid search considering the landing velocity, ΔV upper bound, and $d^\star$, which is shown in figure 3a. If the trajectory constraints are considered together with the assumption that there is a 50 m uncertainty in the position of the SSTO as well, several of the points in the Pareto front can be removed (see figure 3b). These points represent sets of trajectories with similar landing conditions which depart from a region around the SSTO. An example point is shown in figure 4, where it can be seen that there is a dense region of trajectories around a specific point along the SSTO. As a polynomial representation of the dynamics is available, a large number of samples can be taken efficiently to characterise the $\Delta\boldsymbol{V}$ distribution, which is shown in figure 5. As this is a dense region of possible landing trajectories, there is a high likelihood that robust landing trajectories are contained in this region of phase space. Therefore, either the mean of this distribution can be used as the target landing trajectory, or the distributions of deployment positions and $\Delta\boldsymbol{V}$ obtained here can be used to initialise a more refined search of robust ballistic landing trajectories.

5 Robust Landing Design

Using the results from the backwards propagation using GIPA, a more refined search using the distribution of the resulting $\Delta\boldsymbol{V}$ can be performed. As now the forward propagation is used, the GIPA method will not be suitable anymore as parts of the propagated set will likely intersect with the singularity associated with the gravitational force of the secondary body, i.e. the $\frac{\mu}{r_2}$ term. The non-intrusive Chebyshev interpolation (NCI) method is more suited to this problem as it only uses individual points that are propagated up until the time of landing. Nevertheless, the large discontinuity of part of the samples landing and others remaining in ballistic flight can also cause a divergence in the interpolation polynomial. Therefore, the propagation is stopped when a part of the samples have landed.

Another grid search is performed using the bounds of figure 5, where 40 points in the $\Delta\boldsymbol{V}$ Magnitude, elevation $\phi_{\Delta V}$, and azimuth $\theta_{\Delta V}$ are taken. Additionally, 40 deployment times are also considered, centered around the original deployment time t_d, with a quarter of the period of Dimorphos as bounds, i.e. $[t_d \pm \frac{1}{4}T_{Dim}]$. As was discussed in section 1 and shown in figure 1, for a robust tra-

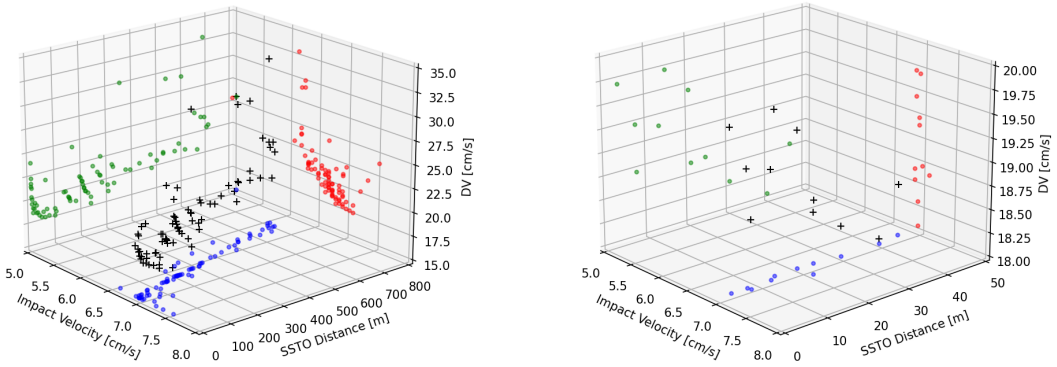

(a) Pareto front from grid search.

(b) Constrained Pareto front from grid search.

Figure 3: Pareto fronts generated from the grid search for the initial trajectory generation. The markers with a "+" sign are the points in the full 3-dimensional objective space, whereas the colored dots are the projections of these points on the 2-dimensional planes.

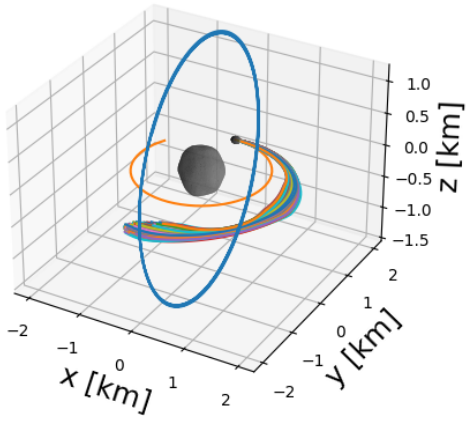

Figure 4: A set of 500 samples taken from the polynomial representing the landing trajectory.

jectory it is important to look at not just the objective variable, but also at its variation as a result of the uncertainties. In this case, the main objective variable that is considered is the distance with respect to the nominal landing location plus its 3σ variation (calculated using the coefficients of the final polynomial). Besides that, the upper bound for the landing velocity and the mean impact angle are also taken into account into the Pareto front. However, for these two variables the variance in these values is not considered. A 0.5 cm/s uncertainty is considered in the velocity magnitude, together with a 1 degree uncertainty in the ΔV angles. As before, a 10 percent uncertainty is also introduced for the gravitational parameter of both bodies.

The resulting Pareto front is shown in figure 6. Most of the points are within the constraints that were discussed in section 4. As the grid search was performed from the region of parameters taken from the backwards propagation method, a relatively large amount of points are found to be within the constraints. Additionally, the landing velocities show some relatively low values which were not considered in the initial backwards grid search. However, most of these are due to the fact the not all parts of the lander set have landed yet due to the necessity of stopping the propagation earlier. Hence, the velocity can increase further in the final ballistic phase of these parts of the set, possibly increasing the velocity.

A specific point from the grid was selected to be investigated further, where a set of 500 samples from this polynomial approximation are shown in figure 7. This point was selected due to the low value of the distance metric and low impact angle. As the distance metric is low, the spread of trajectories at the end of the propagation is relatively small. Additionally, the mean impact angle is quite low, meaning that the mean velocity vector of the set is pointing near perpendicular with respect to the surface of Dimorphos. As time increases, this will also mean that most of the other trajectories which have not (yet) landed will, generally, move towards the direction of the surface of Dimorphos.

To compare the robustness of the resulting trajectory, it is compared with two other methods. The first method is a simple single shooting method from the mean position of the SSTO, not considering any uncertainties. The COBYLA solver [31] was used to obtain the minimum distance ballistic landing trajectory. The second trajec-

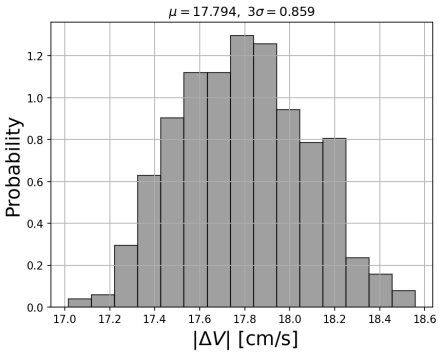

(a) Δ V Magnitude distribution.

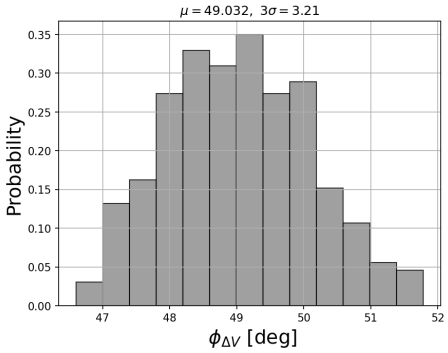

(b) Δ V Elevation angle distribution.

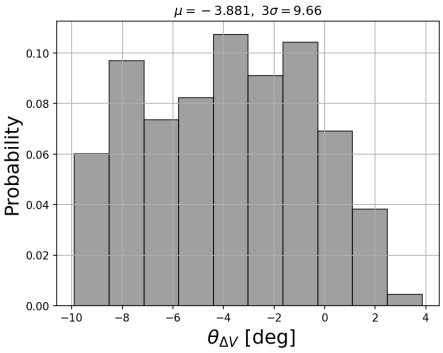

(c) Δ V Azimuth angle distribution.

Figure 5: Δ V distributions taken from sampling the backwards propagated polynomial.

Table 2: Results for different landing trajectories.

Trajectory	Decision Vector	Landing Success (%)
Single, no uncertainty	(17.9538, 48.5128, -3.8786, 2.5539)	51.8
GIPA Backwards	(17.9957, 49.0544, -4.8891, 2.5299)	60.0
NCI Forwards	(17.3077, 49.4872, 3.6410, 3.5903)	78.2

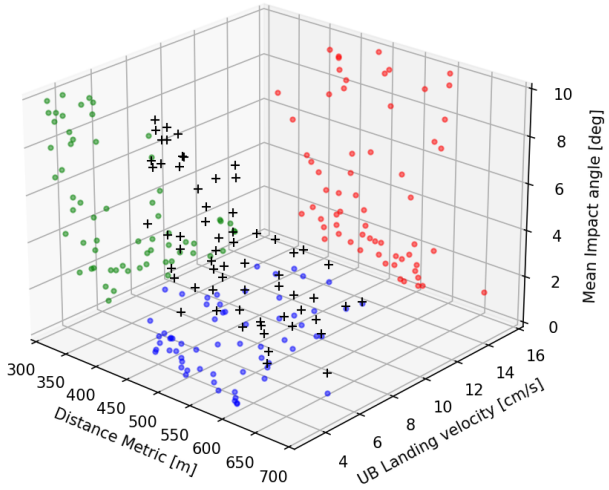

Figure 6: The Pareto front for the NCI forward propagation grid search. The markers with a "+" sign are the points in the full 3-dimensional objective space, whereas the colored dots are the projections of these points on the 2-dimensional planes.

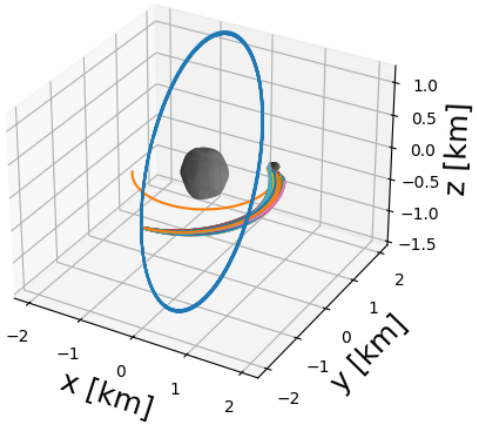

Figure 7: 500 samples from the trajectory with the lowest distance metric.

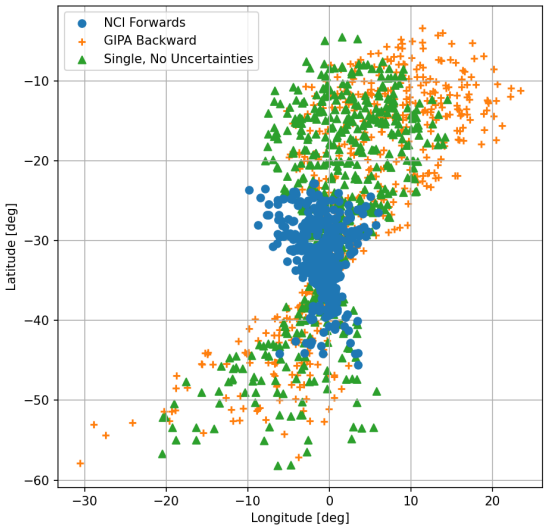

Figure 8: The distribution of the landing locations for the MC analysis of the three cases: no uncertainty shooting result, GIPA backwards propagation method, and the full GIPA + NCI forwards propagation method.

tory is the mean trajectory found from the selected point from the GIPA backwards propagation grid search. This method results in a dense area of landing trajectories, thus this trajectory should be more robust compared to the single shooting method. The resulting trajectory and landing success percentage, measured using a Monte Carlo method, is shown in table 2. The GIPA + NCI trajectory shows a significant increase (about 26 percent increase to a final value of 78.2 percent) in the amount of landings compared with the other two methods. The GIPA only method does increase the robustness compared to the single shooting method, but the refining NCI step significantly increases the performance afterwards. The difference in landing footprint can also be seen in figure 8, where it shows that the NCI method compared to the other two methods significantly reduces the spread of the landing locations.

The difference in the distribution of landing conditions (i.e. the landing velocity and landing angle) can be seen in figure 9. For these results, some of the advantage of the GIPA backwards process can be seen, as it has a lower mean value and upper bound for the velocity and a higher amount of points with (near) perpendicular landings. However, it does produce also a set of points with high impact angles. As the GIPA method propagates from

a region with pre-set desired landing conditions, it is to be expected that the landing conditions would be closer to the desired values compared to the NCI method.

6 Conclusion

This research developed new methods to generate robust ballistic trajectories from the self-stabilized terminator orbit for landing on the secondary of a binary asteroid system. The GIPA backwards propagation method found several feasible trajectories, using a grid search, which intersect with the SSTO. Applying several constraints reduced the amount of possible deployment maneuvers, but several were still available. A specific set of trajectories was investigated in more detail and it was found that this method is able to increase the landing success compared to a simple single shooting trajectory finding method by around 10 percent. However, the success percentage of 60 percent is still not sufficient for most mission operations application. This occurs as there is no perfect overlap between the multivariate distribution of the states of the lander and the distribution of states of the orbiter.

Starting from the distribution of the GIPA backwards propagation method, the NCI forwards propagation method is able to find much more robust trajectories, increasing the success percentage to 78.2 percent. The distributions of landing locations is also much more concentrated compared to the GIPA only method. However, the distribution of landing velocities and angles is found to be less concentrated around the desired values compared to the GIPA method, as this method starts propagating from these desired values and thus more trajectories will end up around those values.

Future research will focus on improving the dynamical model to be more realistic. Including for example non-spherical gravity perturbations and/or Solar radiation pressure. Furthermore, a better trajectory searching approach could be used for the final step, e.g. an optimization method or finer grid size, to be able to improve the found solution even more.

Acknowledgments

The authors would like to acknowledge the ESA OSIP program for partly sponsoring this research project. Furthermore, the authors are grateful to Annalisa Riccardi and Cristian Greco for their insights on the GIPA method.

References

[1] H. Goldberg, o. Karatekin, B. Ritter, A. Herique, P. Tortora, C. Prioroc, B. Gutierrez, P. Martino, and I. Carnelli, "The Juventas CubeSat in Support of ESA's Hera Mission to the Asteroid Didymos," *Small Satellite Conference*, 8 2019. [Online]. Available: https://digitalcommons.usu.edu/smallsat/2019/all2019/73

[2] J. Kawaguchi, "Hayabusa, summary of guidance, navigation and control achievement in its proximity phase," in *Collection of Technical Papers - AIAA/AAS Astrodynamics Specialist Conference, 2006*, vol. 2. American Institute of Aeronautics and Astronautics Inc., 2006, pp. 1334–1341.

[3] P. Muñoz, F. Budnik, V. Companys, B. Godard, C. M. Casas, T. Morley, and V. Janarthanan, "Rosetta navigation during lander delivery phase and reconstruction of Philae descent trajectory and rebound," in *25th International Symposium on Space Flight Dynamics*, 2015.

[4] Y. Tsuda, T. Saiki, F. Terui, S. Nakazawa, M. Yoshikawa, and S. i. Watanabe, "Hayabusa2 mission status: Landing, roving and cratering on asteroid Ryugu," *Acta Astronautica*, vol. 171, pp. 42–54, 6 2020.

[5] D. S. Lauretta, S. S. Balram-Knutson, E. Beshore, W. V. Boynton, C. Drouet d'Aubigny, D. N. DellaGiustina, H. L. Enos, D. R. Golish, C. W. Hergenrother, E. S. Howell, C. A. Bennett, E. T. Morton, M. C. Nolan, B. Rizk, H. L. Roper, A. E. Bartels, B. J. Bos, J. P. Dworkin, D. E. Highsmith, D. A. Lorenz, L. F. Lim, R. Mink, M. C. Moreau, J. A. Nuth, D. C. Reuter, A. A. Simon, E. B. Bierhaus, B. H. Bryan, R. Ballouz, O. S. Barnouin, R. P. Binzel, W. F. Bottke, V. E. Hamilton, K. J. Walsh, S. R. Chesley, P. R. Christensen, B. E. Clark, H. C. Connolly, M. K. Crombie, M. G. Daly, J. P. Emery, T. J. McCoy, J. W. McMahon, D. J. Scheeres, S. Messenger, K. Nakamura-Messenger, K. Righter, and S. A. Sandford, "OSIRIS-REx: Sample Return from Asteroid (101955) Bennu," pp. 925–984, 10 2017. [Online]. Available: https://link-springer-com.proxy.lib.strath.ac.uk/article/10.1007/s11214-017-0405-1

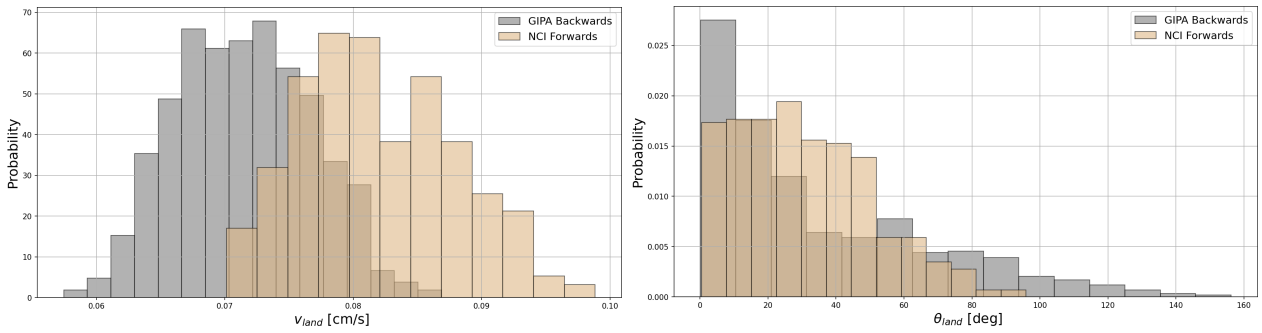

(a) Distribution of landing velocities.

(b) Distribution of landing angles.

Figure 9: The distributions in the landing velocity (left) and impact angles (right) for the cases of the GIPA backwards integration method and the GIPA + NCI forward integration method.

[6] O. Çelik, O. Karatekin, B. Ritter, and J.-P. Sánchez, "Reliability Analysis of Ballistic Landing in Binary Asteroid 65803 (1996GT) Didymos under Uncertainty and GNC Error Considerations," 2017.

[7] S. Tardivel and D. J. Scheeres, "Ballistic deployment of science packages on binary asteroids," *Journal of Guidance, Control, and Dynamics*, vol. 36, no. 3, pp. 700–709, 4 2013. [Online]. Available: https://arc.aiaa.org/doi/abs/10.2514/1.59106

[8] S. Tardivel, P. Michel, and D. J. Scheeres, "Deployment of a lander on the binary asteroid (175706) 1996 FG3, potential target of the european MarcoPolo-R sample return mission," *Acta Astronautica*, vol. 89, pp. 60–70, 8 2013. [Online]. Available: https://www.sciencedirect.com/science/article/pii/S0094576513000799

[9] D. Villegas Pinto, D. Hestroffer, E. Canalias, and F. Capolupo, "Deployment of small-body landers from terminator orbits in perturbed environments," in *AAS/AIAA Astrodynamics Specialist Conference*, Virtual Lake Tahoe, 4 2020.

[10] E. Herrera-Sucarrat, P. L. Palmer, and R. M. Roberts, "Asteroid Observation and Landing Trajectories Using Invariant Manifolds," *Journal of Guidance Control and Dynamics*, vol. 37, no. 3, pp. 907–920, 2014. [Online]. Available: https://openresearch.surrey.ac.uk/esploro/outputs/journalArticle/Asteroid-Observation-and-Landing-Trajectories-Using/99512229002346

[11] O. Çelik, J. P. Sanchez, O. Karatekin, and B. Ritter, "Analysis of natural landing trajectories for passive landers in binary asteroids : A case study for (65803) 1996GT Didymos," *5th Planetary Defence Conference*, no. May, pp. 1–16, 5 2017. [Online]. Available: http://dspace.lib.cranfield.ac.uk/handle/1826/12310

[12] I. Fodde, J. Feng, and M. Vasile, "Robust Trajectory Design for Ballistic Landings on Dimorphos." *AIAA Science and Technology Forum and Exposition, AIAA SciTech Forum 2022*, 2022. [Online]. Available: https://arc.aiaa.org/doi/10.2514/6.2022-1476

[13] F. Ferrari and M. Lavagna, "Ballistic landing design on binary asteroids: The AIM case study," *Advances in Space Research*, vol. 62, no. 8, pp. 2245–2260, 10 2018.

[14] O. Çelik, J. P. Sanchez, O. Karatekin, and B. Ritter, "A comparative reliability analysis of ballistic deployments on binary asteroids," *Acta Astronautica*, vol. 156, pp. 308–316, 3 2019.

[15] D. J. Scheeres, "Orbital mechanics about small bodies," *Acta Astronautica*, vol. 72, pp. 1–14, 3 2012.

[16] X. Jiang and S. Li, "Mars entry trajectory planning using robust optimization and uncertainty quantification," *Acta Astronautica*, vol. 161, pp. 249–261, 8 2019.

[17] Y. Ren and J. Shan, "Reliability-Based Soft Landing Trajectory Optimization near Asteroid with Uncertain Gravitational Field," *Journal of Guidance, Control, and Dynamics*, vol. 38, no. 9, pp. 1810–1820, 7 2015. [Online]. Available: https://arc.aiaa.org/doi/10.2514/1.G000903

[18] "Hera Didymos Reference Model Issue 5," ESA, Tech. Rep., 2020.

[19] K. Wakker, *Fundamentals of Astrodynamics*. Delft: Institutional Repository Delft University of Technology, 1 2015.

[20] F. Ferrari, V. Franzese, M. Pugliatti, C. Giordano, and F. Topputo, "Trajectory Options for Hera's Milani CubeSat Around (65803) Didymos," *The Journal of the Astronautical Sciences*, pp. 1–22, 9 2021. [Online]. Available: https://link.springer.com/article/10.1007/s40295-021-00282-z

[21] H. F. Agrusa, I. Gkolias, K. Tsiganis, D. C. Richardson, A. J. Meyer, D. J. Scheeres, M. Ćuk, S. A. Jacobson, P. Michel, O. Karatekin, A. F. Cheng, M. Hirabayashi, Y. Zhang, E. G. Fahnestock, and A. B. Davis, "The excited spin state of Dimorphos resulting from the DART impact," *Icarus*, vol. 370, p. 114624, 12 2021.

[22] M. Vasile, C. O. Absil, and A. Riccardi, "Set propagation in dynamical systems with generalised polynomial algebra and its computational complexity," *Communications in Nonlinear Science and Numerical Simulation*, vol. 75, pp. 22–49, 8 2019.

[23] A. Riccardi, C. Tardioli, and M. Vasile, "An intrusive approach to uncertainty propagation in orbital mechanics based on tchebycheff polynomial algebra," in *Advances in the Astronautical Sciences*, vol. 156. Vail: Univelt Inc., 2016, pp. 707–722.

[24] M. Valli, R. Armellin, P. Di Lizia, and M. R. Lavagna, "Nonlinear filtering methods for spacecraft navigation based on differential algebra," *Acta Astronautica*, vol. 94, no. 1, pp. 363–374, 1 2014.

[25] D. Pérez-Palau, J. J. Masdemont, and G. Gómez, "Tools to detect structures in dynamical systems using Jet Transport," *Celestial Mechanics and Dynamical Astronomy*, vol. 123, no. 3, pp. 239–262, 11 2015. [Online]. Available: https://link.springer.com/article/10.1007/s10569-015-9634-3

[26] C. O. Absil, A. Riccardi, M. Vasile, and C. Tardioli, "SMART-UQ: uncertainty quantification toolbox for generalised intrusive and non intrusive polynomial algebra," in *6th International Conference on Astrodynamics Tools and Techniques*, Darmstadt, Germany, 3 2016. [Online]. Available: https://pureportal.strath.ac.uk/en/publications/smart-uq-uncertainty-quantification-toolbox-for-generalised-intru

[27] Y. z. Luo and Z. Yang, "A review of uncertainty propagation in orbital mechanics," *Progress in Aerospace Sciences*, vol. 89, pp. 23–39, 2 2017.

[28] C. Tardioli, M. Kubicek, M. Vasile, E. Minisci, and A. Riccardi, "Comparison of non-intrusive approaches to uncertainty propagation in orbital mechanics," in *Advances in the Astronautical Sciences*, vol. 156, 2016, pp. 3979–3992.

[29] I. Fodde, J. Feng, and M. Vasile, "Uncertainty maps for motion around binary asteroids," *Celestial Mechanics and Dynamical Astronomy 2022 134:5*, vol. 134, no. 5, pp. 1–23, 8 2022. [Online]. Available: https://link.springer.com/article/10.1007/s10569-022-10096-2

[30] J. M. Hedo, M. Ruíz, and J. Peláez, "On the minimum orbital intersection distance computation: a new effective method," *Monthly Notices of the Royal Astronomical Society*, vol. 479, no. 3, pp. 3288–3299, 9 2018. [Online]. Available: https://academic.oup.com/mnras/article/479/3/3288/5039662

[31] M. J. D. Powell, "A Direct Search Optimization Method That Models the Objective and Constraint Functions by Linear Interpolation," *Advances in Optimization and Numerical Analysis*, pp. 51–67, 1994. [Online]. Available: https://link.springer.com/chapter/10.1007/978-94-015-8330-5_4